Available online at www.sciencedirect.com

SciVerse ScienceDirect

Ceramics International 39 (2013) 3027–3034

CERAMICS INTERNATIONAL

www.elsevier.com/locate/ceramint

Surface modification of nanocrystalline calcium phosphate bioceramic by low energy nitrogen ion implantation

K. Thanigaiarul[a], K. Elayaraja[a], P. Magudapathy[b], U. Kamachi Mudali[c], K.G.M. Nair[b], M. Sudarshan[d], J.B.M. Krishna[d], A. Chakraborty[d], S. Narayana Kalkura[a,*]

[a]*Crystal Growth Centre, Anna University, Chennai, Tamil Nadu, India*
[b]*Accelerator Material Science Section, Material Science Group, Indira Gandhi Centre for Atomic Research, Kalpakkam, Tamil Nadu, India*
[c]*Metallurgy and Materials Group, Indira Gandhi Centre for Atomic Research, Kalpakkam, Tamil Nadu, India*
[d]*University Grants Commission, Department of Atomic Energy, Consortium for Scientific Research, Kolkata, West Bengal, India*

Received 6 August 2012; received in revised form 20 September 2012; accepted 21 September 2012
Available online 17 October 2012

Abstract

The microwave synthesized hydroxyapatite (HAp-$Ca_{10}(PO_4)_6(OH)_2$, 35 nm) was implanted with 30 keV nitrogen ion (N^+) with fluences of 1×10^{15}, 1×10^{16} and 1×10^{17} ions/cm^2. The samples were characterized by GIXRD (Glancing Incidence X-ray Diffraction) and atomic force microscopy along with measurement of resistivity, permittivity, ac (alternating current) conductivity, photoluminescence, wettability and *in vitro* bioactivity. Implantation did not cause any appreciable change in crystallite size and lattice parameters. The ion implanted samples revealed enhanced permittivity, ac conductivity, photoluminescence and average pore size (50%), whereas there was a significant decrease in resistivity, surface roughness, and wettability. The *in vitro* bioactivity and protein absorption were found to improve on nitrogen ion implantation.

Keywords: A. Implantation; Bioactivity; Hydroxyapatite; Wettability

1. Introduction

The main inorganic mineral constituent of bones and teeth is HAp, which belongs to the family of apatites. HAp is considered as an ideal material for hard tissue replace'ment due to its biocompatibility and high thermal stability [1]. Bulk HAp is used as bone cement, protein adsorbent, gas sensors and as a chromatographic agent [2]. There are some limitations on using metallic implants with HAp coating as it causes inflammation, integration problems and mishandling [3]. The surface properties of implant materials such as surface roughness, surface potential, and wettability play a vital role in binding to the living cells [4]. The surface of the implant materials can be modified by treatments such as laser irradiation [5], electron [6], plasma and ion implantation [7] and irradiation [8]. Ion beam implantation is employed to modify the surface of solid thin films [9] and polymers [10,11]. Low energy ion implantation provides selective surface modification and thereby enhances the osseointegration, cell adhesion, proliferation and haemocompatibility [12,13] without affecting the bulk properties of the materials. Further, ion implantation could be used to modify the surface chemistry and regulate the depth of penetration and the dose. The swift heavy ion (SHI) irradiation on HAp had enhanced the *in vitro* bioactivity [8–14]. Pelletier et al. studied the effect of high energy (1–1.5 MeV) implantation of nitrogen and argon ions to improve the mechanical properties of HAp thin film [15]. Irradiation of low energy argon ion (0.6–1.2 kV) and high energy oxygen ion (2 MeV) lead to enhanced luminescence, wettability, bioactivity and cell adhesion [16,17].

Here we report the effect of low energy nitrogen ion implantation on microwave synthesized HAp and qualitatively

*Corresponding author. Tel.: +91 44 22208335.
E-mail addresses: kalkurasn@annauniv.edu, kalkura@yahoo.com (S.N. Kalkura).

0272-8842/$ - see front matter © 2012 Elsevier Ltd and Techna Group S.r.l. All rights reserved.
http://dx.doi.org/10.1016/j.ceramint.2012.09.081

discuss the role of implantation in tailoring resistivity, permittivity, ac conductivity and photoluminescence, less wettability and in vitro bioactivity.

2. Materials and method

Nanocrystalline HAp was synthesized by microwave synthesis technique using analytical grade reagents of calcium nitrate tetrahydrate ($Ca(NO_3)_2.4H_2O$, Merck), diammonium hydrogen phosphate ($(NH_4)_2.HPO_4$, Merck), and ammonia solution (MERCK). 0.6 M diammonium hydrogen phosphate was dissolved in deionized water and the pH of the solution was adjusted to 10 using ammonia solution. 1.0 M calcium nitrate tetrahydrate was added drop by drop to diammonium hydrogen phosphate solution with continuous stirring and pH of the solution was maintained at 10. The solution was further stirred vigorously for 2 h at room temperature at constant pH-10. Subsequently the precipitated solution was subjected to microwave irradiation (household microwave oven −900 W and 2.45 GHz) for about 30 min. The white precipitate was washed with deionized water and dried in hot air oven at 80 °C.

The collected powder was pressed into circular pellets (8 mm diameter and 1 mm thickness). After annealing of pellets at 200 °C for 2 h, the samples were subjected to ion implantation. Implantation was carried out at the AMSS, IGCAR, Kalpakkam using 150 kV accelerator. 30 keV nitrogen ions were implanted with a charge state of 1^+ on HAp with fluences 1×10^{15}, 1×10^{16} and 1×10^{17} ions/cm^2 and these samples will be referred to as 1HAp, 2HAp and 3HAp, respectively. The ion beam current of about 300–400 nA was maintained during implantation. The dimension of the ion beam implanted area was 12 mm × 12 mm. The projected range of nitrogen ions in hydroxyapatite was 145.4 nm calculated by using the stopping and range of ions in matter (SRIM –version 2008).

GIXRD analysis was performed on the samples using the STOE diffractometer having Cu K_α (0.1540 nm) radiation with a fixed glancing angle of 1°. The slit width of 0.3 mm was used with a scan speed of 0.05°/min. It was operated at maximum voltage of 40 kV/40 mA. Resistivity was measured using four probe setup. Real part of relative permittivity and ac conductivity of the samples were measured from complex impedance measurement done in a frequency (f) range of 0.1 Hz to 1 MHz using Alpha—a high performance frequency analyzer from Novo control Technologies. The Photoluminescence studies were done using Horiba Jobin Yvoun spectrofluorometer at an excitation wavelength of 325 nm.

The surface morphology of the sample was analyzed by atomic force microscopy (AFM, NT-MDT-SOLVER PRO EC system) and scanning electron microscopy (F E I Quanta FEG 200—High Resolution Scanning Electron Microscope).

Wettability was determined by measuring the contact angle with a sessile drop of deionized water (5 μl) deposited on the sample surface at room temperature (27 °C). Euromex optical microscope with inbuilt color charge coupled device (CCD) camera was used for the wettability study. For every fifteen seconds up to 3 min a profile photograph of sessile drop wetting was taken and contact angles were analyzed using imageJ software.

Simulated body fluid (SBF) was used to check the *in vitro* bioactivity. Chemical reagents were dissolved in the order NaCl, $NaHCO_3$, KCl, $NaHPO_4.2H_2O$, $MgCl_2.6H_2O$, $CaCl_2.2H_2O$, Na_2SO_4, Tris buffer and 1 M HCl in deionized water. Subsequently, HCl was used to adjust the pH of the solution to 7.4 at 37 °C [18]. Then the samples were immersed in 20 ml of SBF for a period of three weeks and the solution was renewed once in two days.

3. Results and discussion

The implanted ion loses its energy through interactions with electrons and atomic nuclei of HAp. The projected range of 30 keV N^+ ions into the pellet was 145 nm. The electronic and nuclear energy losses were calculated as 0.821 keV/nm and 0.684 keV/nm, respectively using SRIM-2008 program [19]. In this circumstance, electronic energy losses play a predominant role compared to the nuclear energy loss.

3.1. GIXRD

The GIXRD pattern of pristine, 1HAp, 2HAp and 3HAp samples was as shown in Fig. 1. All samples showed the presence of pure phase of HAp and the peak positions were in good agreement with JCPDS data (09-0432). The crystallite size and lattice parameters were determined using the software, MAUD (Material Analysis Using Diffraction) (Table 1). There was no significant change in crystallite size, lattice parameters and unit cell volume on N^+ ion implantation (Table 1). The defects formed due to implantation could occupy interstitial positions and therefore might not considerably modify the crystallite size, lattice parameters and unit cell volume [14].

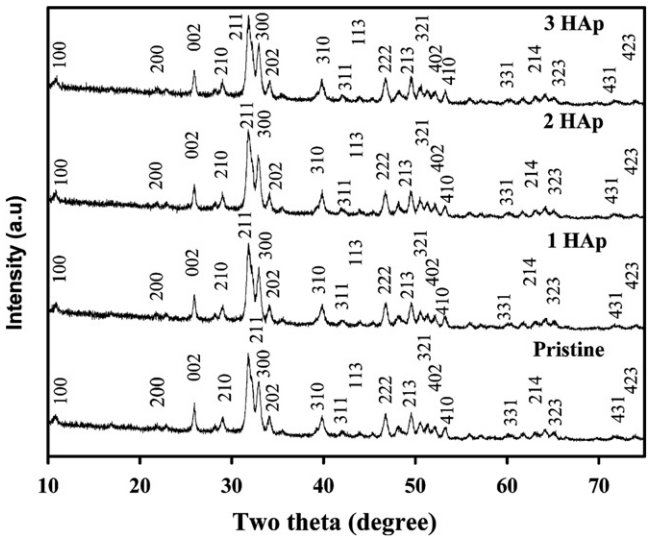

Fig. 1. The XRD pattern of pristine, 1HAp, 2HAp, 3HAp samples.

3.2. Resistivity

The resistivity of pristine, 1HAp, 2HAp and 3HAp was 94×10^3, 47×10^3, 31.33×10^3 and 23.5×10^3 Ωm, respectively (Fig. 2). There was 75% decrease of resistivity in 3HAp when compared to pristine. As nitrogen ion fluence augment, resistivity decreased, possibly due to the production of defects in the sample. The resistivity was tailored by N^+ ion implantation and could lead to non linear resistivity versus ion fluence. Even though the defects were at 145 nm as calculated using SRIM-2008, the surface chemistry might have been modified. During N^+ ion implantation, there was a possibility of generation of O^{2-} and H^+ ions due to localized heating. As ion fluence enhances, resistivity was significantly diminished due to the influence of the conducting ions (O^{2-} and H^+) in the material [20,21].

Table 1
Crystallite size, lattice parameter and volume of the unit cell of pristine, 1HAp, 2HAp, 3HAp.

Sample	Crystallite size (±0.98 nm)	Lattice parameter (Å)		Volume of unit cell (Å)^3
		a	c	
Pristine	36.61	9.429	6.886	530.2
1HAp	34.82	9.443	6.893	531.6
2HAp	36.98	9.431	6.886	530.4
3HAp	36.66	9.431	6.886	530.4

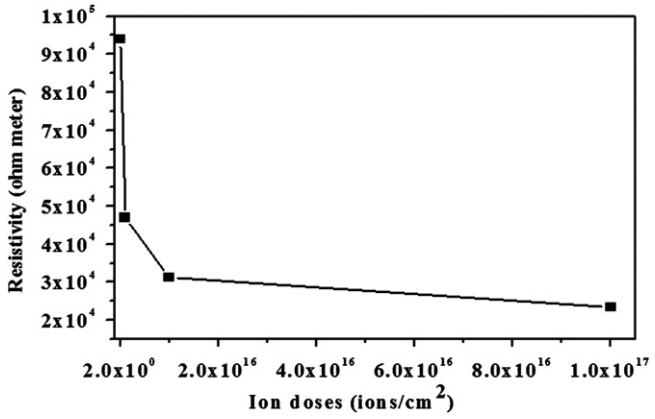

Fig. 2. Measurement of resistivity versus ion doses.

3.3. Permittivity and ac conductivity

The variation in the real part of relative permittivity (ε′) as a function of frequency for pristine and implanted samples was shown in Fig. 3(a). The sample exhibited a frequency-dependent real part of relative permittivity and was found to decrease with increase in frequency. The enhancement of magnitude of permittivity at lower frequency may be due to the raised ionic polarization. At higher frequency, permittivity might have reduced due to the lagging of dipole oscillation and further the space charge did not sustain with the applied electric field. The formation of mobile thermal defects at high temperature and the proton conduction transported along the OH^- chain could lead to a raise in permittivity [22–24].

The ac conductivity of the samples was as shown in Fig. 3(b). The ac conductivity, enhanced gradually with increase in frequency. At lower frequency, the observed low conductivity of the samples could be due to the sluggish turn around of the ions with the electric field. At higher frequency, the ac conductivity was found to be enhanced in the implanted sample, possibly due to the intricate arrangement of conducting ions and proton skipping along *c*-axis linking O^{2-} anion or OH^- [25,26]. The enhanced ionic polarization of N^+ ion implanted samples may increase the calcification and mineralization of bone tissues at the fracture site and subsequently lead to a faster rate of bone growth [27].

3.4. Photoluminescence

The photoluminescence (PL) of the samples excited at wavelength λ_{ex} = 325 nm was as shown in Fig. 4. The wavelength of the emitted light was in the range of 400 nm to 600 nm and emission peaks at 456 nm and 554 nm were observed for all the samples. The PL spectrum of pristine was broad with a band gap energy of 2.72 eV (Fig. 4(a)) possibly

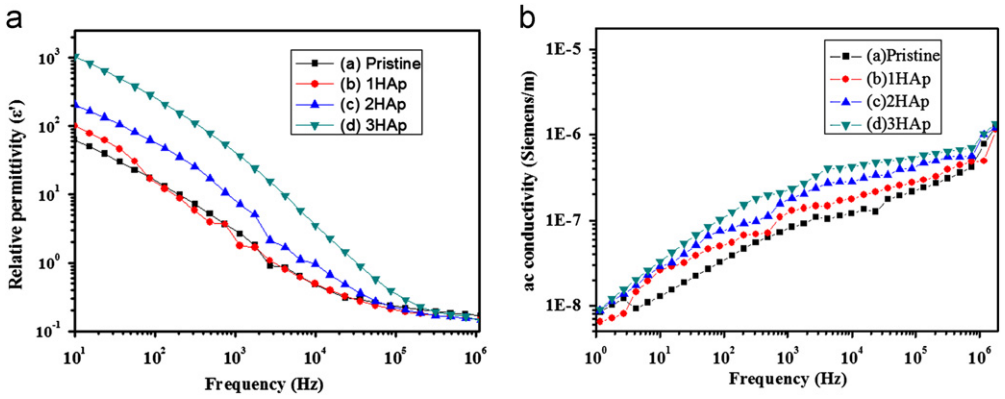

Fig. 3. (a) The real part of relative permittivity (ε′) as a function of frequency for (a) Pristine, (b) 1HAp, (c) 2HAp and (d) 3HAp samples. (b) The ac conductivity as a function of frequency for (a) Pristine, (b) 1HAp, (c) 2HAp and (d) 3HAp samples.

due to the deep energy level in the sample. On N^+ ion implantation, the intensity of PL spectrum was enhanced, without any change in the band gap energy as shown in Fig. 4(b–d), due to the increase in defect's energy levels, recombination of electron and hole pair and diffusivity of N^+ ion [28,29]. Yang et al. reported red luminescence attributed to the charge transfer transition in the material [30]. The enhanced photoluminescence of the implanted samples might help in the fabrication of a biosensor for *in-situ* monitoring of new bone growth [31].

3.5. Atomic force microscope and scanning electron microscope

The surface topography of the pristine and implanted samples was as shown in Fig. 5(a–d). The surface roughness and the average pore size of the pristine sample were 100 nm and 1.90 μm, respectively. There was a decrease in average roughness on implantation compared to the pristine (Fig. 5(a–d), Table 2). At lower fluence, the average

Table 2
AFM analyses of the pristine and implanted samples.

Sample	Average roughness (± 1 nm)	Average pore size (± 1 μm)
Pristine	160	1.90
1HAp	85.03	4.27
2HAp	97.93	2.79
3HAp	80.21	2.07

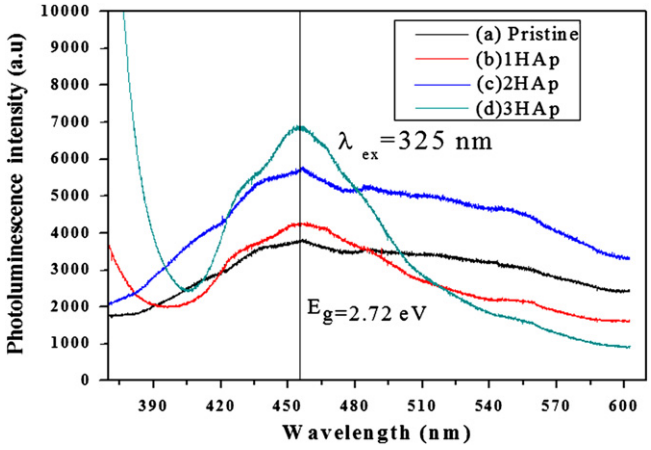

Fig. 4. Photoluminescence of (a) pristine, (b) 1HAp, (c) 2HAp and (d) 3HAp samples.

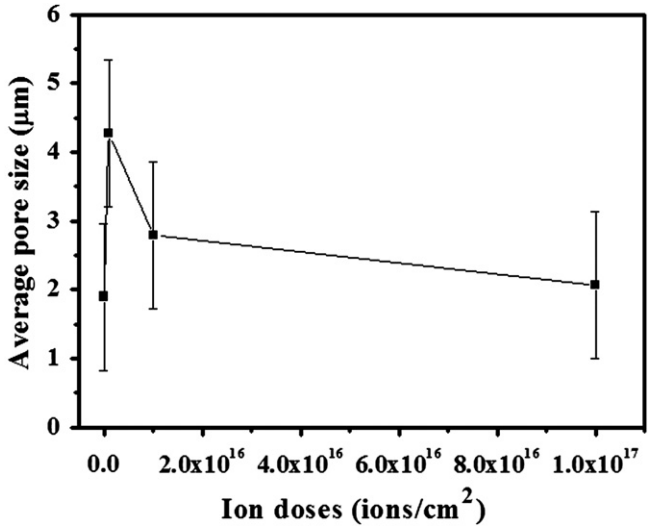

Fig. 6. Average pore size versus ion doses.

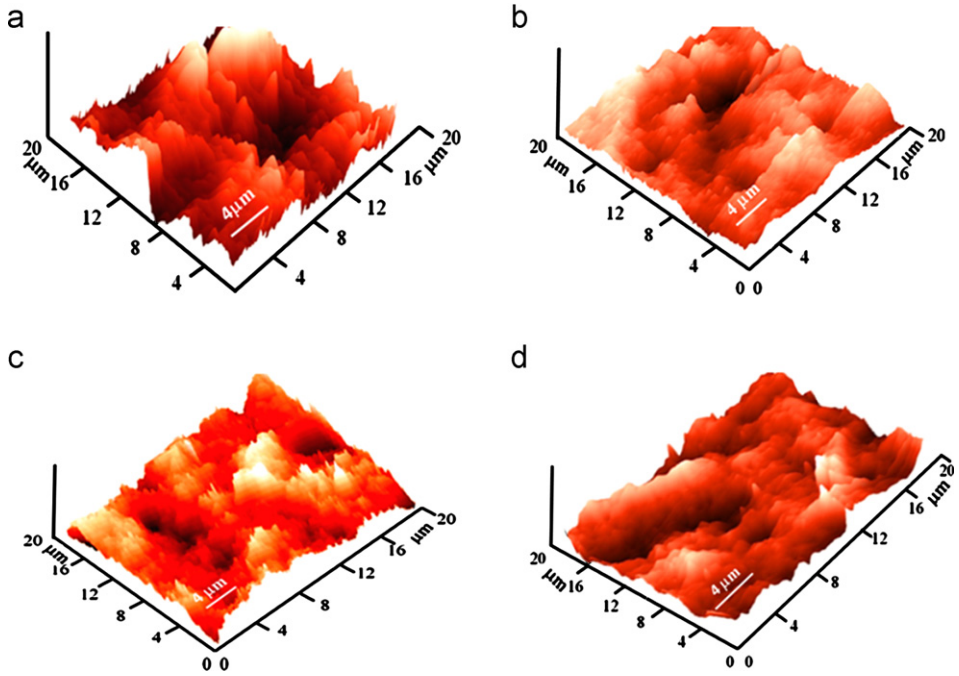

Fig. 5. AFM 3D images of (a) Pristine, (b) 1HAp, (c) 2HAp and (d) 3HAp samples.

pore size was enhanced considerably. Subsequently, as the ion fluence increases, the average pore size seems to be decreased due to the local heating leading to the melting of the surface [32]. The variation of average pore size versus ion doses was shown as in Fig. 6. The reduction in surface roughness of N^+ implanted samples, observed could be due to the sputtering of atoms on the surface in addition to the ion induced surface diffusion [33].

The pristine sample revealed homogeneous smooth surface (Fig. 7(a)). At low fluence (1HAp), elongated pores were observed (4.27 μm) (Fig. 7(b)). Agglomerated particles (3 μm) were revealed on the surface of 2HAp (Fig. 7(c)). At higher fluence (3HAp), the surface became textured as shown in (Fig. 7(d)). The variation in surface morphology of the N^+ ion implanted sample might be due to sputtering of atoms and thermal fluctuation in the HAp matrix [33].

3.6. Wettability

Wettability of the sample was determined by measuring the contact angle (Fig. 8(a–d)). The contact angle of pristine was $30 \pm 3^\circ$, revealing a hydrophilic surface. The 1HAp, 2HAp and 3HAp exhibited weak hydrophilic surface with respective contact angles of $74 \pm 3^\circ$, $81 \pm 3^\circ$ and $68 \pm 3^\circ$. The increase in contact angle of the N^+ ion implanted samples could be due to the changes in surface roughness, pore size and polar component of surface

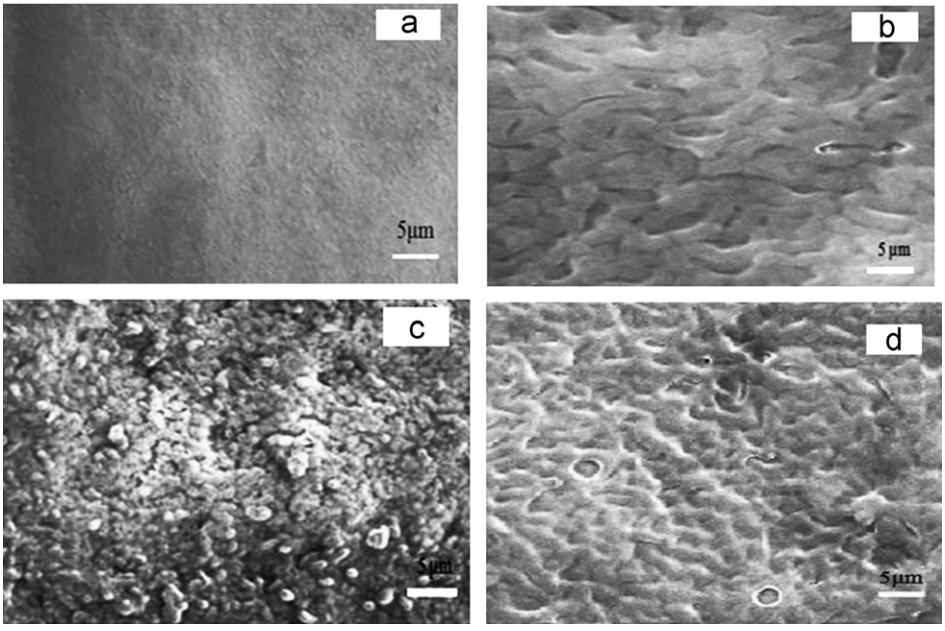

Fig. 7. SEM micrograph of (a) pristine, (b) 1HAp, (c) 2HAp and (d) 3HAp samples.

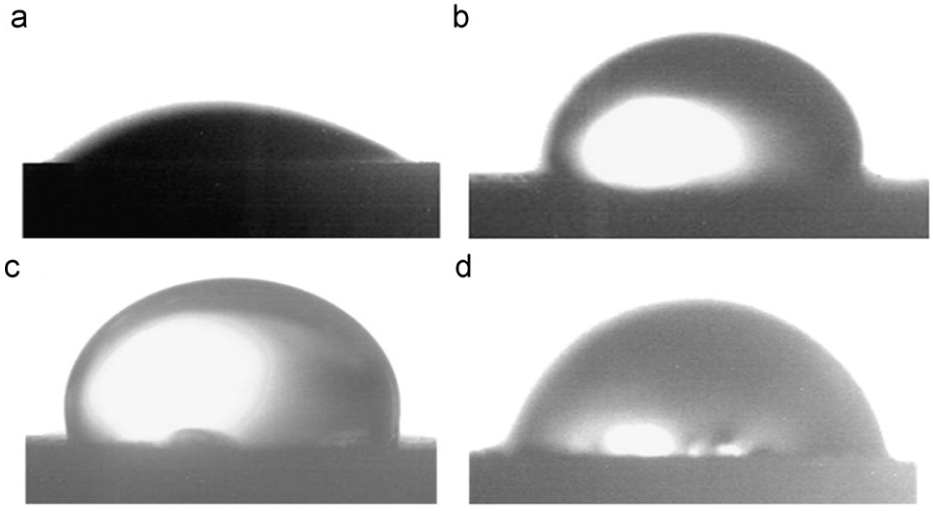

Fig. 8. Different wettability states of (a) pristine, (b) 1HAp, (c) 2HAp and (d) 3HAp samples.

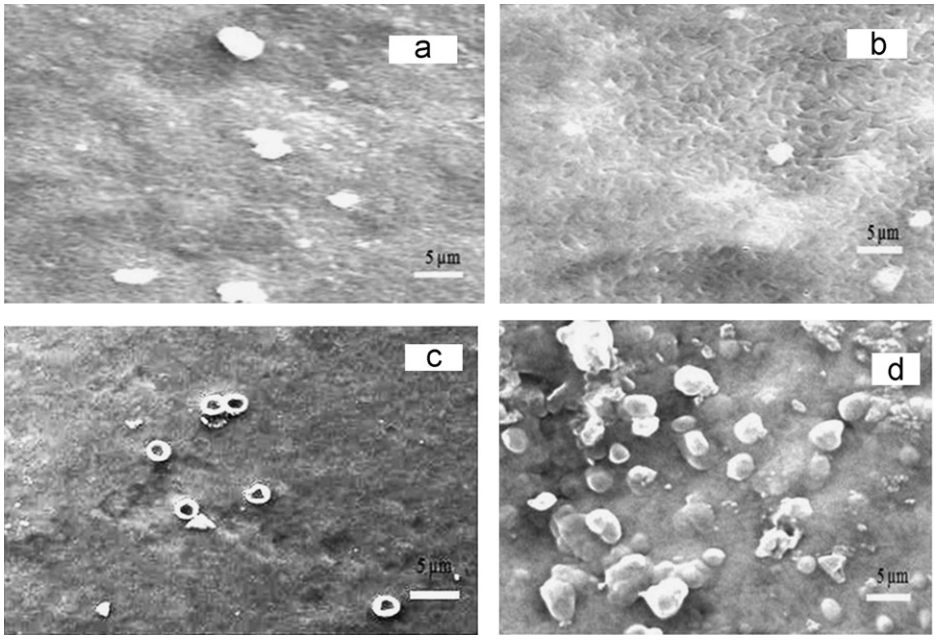

Fig. 9. SEM micrograph of the SBF soaked sample with HAp layer deposited on the surface of (a) pristine, (b) 1HAp, (c) 2HAp and (d) 3HAp samples.

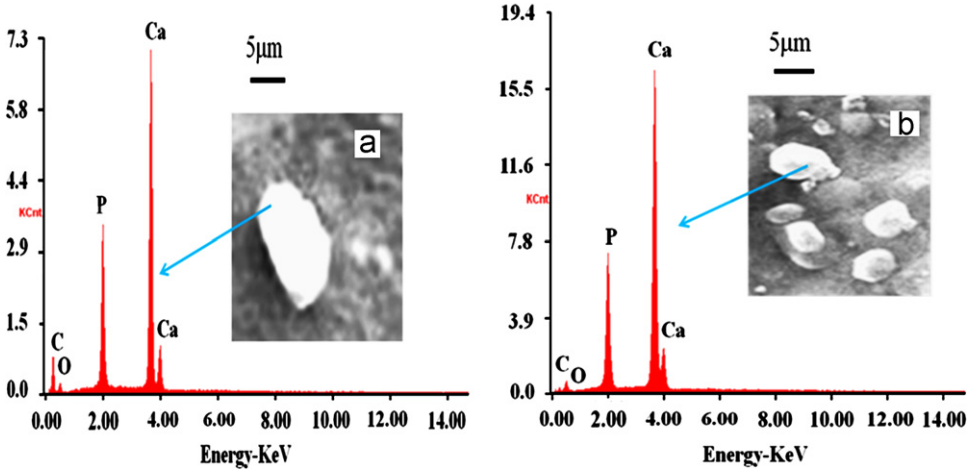

Fig. 10. EDX spectra shows the elemental composition measured on SBF tested (a) pristine and (b) 3HAp sample.

energy, surface chemistry for the reduction in wettability. [34–36] The pristine exhibits, better wettability than the implanted sample and could assist DNA absorption, due to the presence of phosphate groups in the backbone of DNA. The weak hydrophilic surface of the implanted sample might favour the absorption of proteins (Bovine Serum Albumin) that contain hydrophobic part which could easily attach to the hydrophobic implanted surface [37].

3.7. *In vitro* bioactivity

The surface of SBF soaked samples in Fig. 9(a–d). At higher fluence, spherical and agglomerated apatites were formed on the surface. The EDX spectra confirmed the enhanced apatite deposition at a higher fluence (3HAp, Ca/P=2.23) compared with pristine (Ca/P=1.9) (Fig. 10 (a and b)). On implantation, the bioactivity of the samples were increased, possibly due to the improved surface charge and surface energy compared with the pristine and the samples implanted at low fluences [34]. It was reported that oxygen ion irradiation on hydroxyapatite enhanced the *in vitro* bioactivity due to the increase in negative surface charge which attract calcium ion and make the surface layer positive changed. This in turn attracts phosphate ions leading to the deposition of an apatite layer [14,17,37].

4. Conclusions

The effect of implanted nitrogen ion on microwave synthesized nano crystalline HAp was investigated.

The low energy implantation did not cause any change in crystallite size and lattice parameter on implantation. The N^+ ion implantation leads to decreased resistivity and surface roughness. The enhanced permittivity and ac conductivity of implanted samples might improve bone fracture healing and the rate of bone growth. The photoluminescence of ion implanted samples was increased. The decreased wettability of implanted samples could help in the absorption of proteins (BSA). The *in vitro* bioactivity was enhanced by low energy ion implantation. The porosity of the samples could be engineered by this method. Hence this technique is the best tool to modify the surface and tailor the properties such as electrical, photoluminescence, protein absorption and bioactivity of the biomedical implants.

Acknowledgments

The authors thank UGC-DAE CSR, Kolkata for financial support through research project file number (UGC-DAE-CSR-KC/CRS/2009/TE-07/1545) and thank AMSS, IGCAR, Kalpakkam providing facility to carry out ion implantation work. The authors would like to thank for Dr. S.C. Vanithakumari of CSTG, IGCAR, Kalpakkam for AFM studies.

References

[1] M. Vallet-Regi, J.M. Gonsalez-Calbet, Calcium phosphates as substitution of bone tissues, Progress in Solid State Chemistry 32 (2004) 1–31.

[2] J.R. Woodard, A.J. Hilldore, S.K. Lan, C.J. Park, A.W. Morgan, J.A.C. Eurell, S.G. Clark, M.B. Wheeler, R.D. Jamison, A.J.W. Johnson, The mechanical properties and osteoconductivity of hydroxyapatite bone scaffolds with multi-scale porosity, Biomaterials 28 (2007) 45–54.

[3] K.A. Lai, C.H. Chen, C.Y. Yang, W.P. Hu, Failure of hydroxyapatite-coated acetabular cups, Journal of Bone and Joint Surgery, British 84B (2002) 641–646.

[4] Y. Nishi, H. Izumi, J. Kwano, K. Oguri, Y. Kawaguchi, M. Ogata, A. Tonegawa, K. Takayama, T. Kawai, M. Ochi, Effect of electron-beam irradiation on water wettability of, hydroxyapatites for artificial bone, Journal of Materials Science 32 (1997) 3637–3639.

[5] L. Pramatarova, E. Pecheva, T. Petrov, A. Kondyurin, R. Pramatarova, N. Minkovaski, Ion beam and laser processing for hydroxyapatite formation, Vacuum 76 (2004) 339–342.

[6] D. Aronov, G. Rosenman, Trap state spectroscopy studies and wettability modification of hydroxyapatite nanobioceramics, Journal of Applied Physics 101 (2007) 034701.

[7] C.M. Lopatin, T.L. Alford, V.B. Pizziconi, M. Kuan, T. Laursen, Ion beam densification of thin film, Nuclear Instruments and Methods B 145 (1998) 522–531.

[8] E.K. Girija, S.P. Parthiban, R.V. Suganthi, K. Elayaraja, M.I.A. Joshy, R. Vani, P. Kularia, K. Asokan, D. Kanjilal, Y. Yokogawa, S. Narayana kalkura, High energy irradiation a tool for enhancing the bioactivity of Hydroxyapatite, Journal of the Ceramic Society of Japan 116 (2008) 320–324.

[9] H. Pelletier, V. Nelea, P. Mille, Nano-scratch study of pulsed laser-deposited hydroxyapatite thin films implanted at high energy with N^+ and Ar^+ ions, Journal of Materials Science 39 (2004) 4185–4192.

[10] J. Zhanga, X. Yua, H. Lia, X. Liub, Surface modification of polytetrafluoroethylene by nitrogen ion implantation, Applied Surface Science 185 (2002) 255–261.

[11] E. Balanzat, N. Betz, S. Bouffard, Swift heavy ion modification of polymers, Nuclear Instruments and Methods in Physics Research Section B 105 (1995) 46–54.

[12] A.M. Ektessabi, Ion beam processing of bio-ceramics, Nuclear Instruments and Methods in Physics Research Section B 99 (1995) 610–613.

[13] G. Liu, J.W Talley, C. Na, S.L. Larson, L.G. Wolfe, Copper doping improves hydroxyapatite sorption for arsenate in simulated groundwaters, Environmental Science and Technology 44 (2010) 1366–1372.

[14] S. Prakash Parthiban, R.V. Suganthi, E.K. Girija, K. Elayaraja, P.K. Kulriya, Y.S. Katharria, F. Singh, I. Sulania, A. Tripathi, K. Asokan, D. Kanjilal, S. Yadav, T.P. Singh, Y. Yokogawa, S. Narayana Kalkura, Effect of swift heavy ion irradiation on hydrothermally synthesized hydroxyapatite ceramics, Nuclear Instruments and Methods in Physics Research Section B 266 (2008) 911–917.

[15] H. Pelletier, V. Nelea, P. Mille, D. Muller, Mechanical properties of pulsed laser-deposited hydroxyapatite thin films implanted at high energy with N^+ and Ar^+ ions. Part II: nano-scratch tests with spherical tipped indenter, Nuclear Instruments and Methods in Physics Research Section B 216 (2004) 275–280.

[16] A.R. Ananda Sagari, P. Rahkila, M. Vaisanen, R. Lehto, T. Sajavaara, S. Gorelick, M. Laitinen, M. Putkonen, S. Sangyuenyongpipat, J. Timonen, S. Cheng, H.J. Whitlow, Wettability and compositional analysis of hydroxyapatite films modified by low and high energy ion irradiation, Nuclear Instruments and Methods B 266 (2008) 2515.

[17] R.V. Suganthi, S. Prakash Parthiban, K. Elayaraja, E.K. Girija, K. Kulariya, Y.S. Katharria, F. Singh, K. Asokan, D. Kanjilal, S. Narayana Kalkura, Investigations on the in vitro bioactivity of swift heavy oxygen ion irradiated hydroxyapatite, Journal of Materials Science Materials in Medicine 20 (2009) 271.

[18] T. Kokubo, H. Takadama, How useful is SBF in predicting in vivo bone bioactivity, Biomaterials 27 (2006) 2907–2915.

[19] SRIM and TRIM software, ⟨http://www.srim.org⟩.

[20] A. Nikolaev, E.M. Oks, K. Savkin, G.Y. Yushkov, D.J. Brenner, G. Johnson, G.R. Pehrson, I.G. Brown, R.A. Macgill, Surface resistivity tailoring of ceramic insulators for an ion microprobe application, Surface and Coatings Technology 201 (2007) 8120–8122.

[21] V.I. Gushenets, A.G. Nikolaev, E.M. Oks, K.P. Savkin, G.Yu. Yushkov, I.G. Brown, High-energy metal ion implantation for reduction of surface resistivity of alumina ceramic, Review of Scientific Instruments 83 (2012) 02B908.

[22] V.P. Orlovskii, N.A. Zakharov, A.A. Ivanov, Structural transition and dielectric characteristics of high-purity hydroxyapatite, Inorganic Materials 32 (1996) 654–656.

[23] NA. Zakharov, VP. Orlovskii, Dielectric characteristics of biocompatible Ca_{10} $(PO_4)_{(6)}$ $(OH)_{(2)}$ ceramics, Technical Physics Letters 27 (2001) 629–631.

24] K. Yamashita, K. Kitagaki, T. Umegaki, Thermal-instability and proton conductivity of ceramic hydroxyapatite at high-temperatures, Journal of the American Ceramic Society 78 (1995) 1191–1197.

[25] M. Nagai, T. Nishino, Surface conduction of porous hydroxyapatite ceramics at elevated-temperatures, Solid State Ionics 28 (1988) 1456–1461.

[26] M. Sh Kalil, H.H. Beheri, WIA. Fattah, Structural and electrical properties of zirconia/hydroxyapatite porous composites, Ceramics International 28 (2002) 451–458.

[27] G. Scott, J.B. King., A prospective double-blind trial of electrical capacitive coupling in the treatment of nonunion of long bones, Journal of Bone and Joint Surgery, Am 76A (1994) 820–826.

[28] G. Rosenman, D. Aronov, L. Oster, J. Haddad, G. Mezinskis, I. Pavlovska, M. Chaikina, A. Karlov, Photoluminescence and surface photovoltage spectroscopy studies of hydroxyapatite nano-bio-ceramics, Journal of Luminescence 122–123 (2007) 936–938.

[29] R.S. Andre, E.C. Paris, M.F.C. Gurgel, I.L.V. Rosa, C.O. Paiva-Santos, M.S. Lie, J.A. Varela, E. Longo, Structural evolution of

Eu-doped hydroxyapatite nanorods monitored by photoluminescence emission, Journal of Alloys and Compounds 531 (2012) 50–54.
[30] C. Yang, P. Yang, W. Wang, S. Gai, J. Wang, M. Zhang, J. Lin, Synthesis and characterization of Eu-doped hydroxyapatite through a microwave assisted microemulsion process, Solid State Sciences 11 (2009) 1923–1928.
[31] S. Sirivisoot, T.J. Webster, Multiwalled carbon nanotubes enhance electrochemical properties of titanium to determine *in situ* bone formation, Nanotechnology 19 (2008) 295101.
[32] A. Kumar, D. Saikia, F. Singh, D.K. Avasthi, Li^{3+} ion irradiation effects on ionic conduction in P(VDF-HFP)-(PC+DEC)-$LiClO_4$ gel polymer electrolyte system, Solid State Ionics 177 (2006) 2575–2579.
[33] J.S. Lee, J.H. Lee, Surface roughness behaviour of ion irradiated industrial steel, Surface and Coatings Technology 196 (2005) 358–363.
[34] K. Elayaraja, M.I. Ahymah Joshy, R.V. Suganthi, S. Narayana Kalkura, M. Palanichamy, M. Ashok, V.V. Sivakumar, P.K. Kulriya, I. Sulania, D. Kanjilal, K. Asokan, 125 MeV Si^{9+} ion irradiation of calcium phosphate thin film coated by rf-magnetron sputtering technique, Applied Surface Science 257 (2011) 2134–2141.
[35] J. Lawrence, L. Hao, H.R. Chew, On the correlation between Nd:YAG laser-induced wettability characteristics modification and osteoblast cell bioactivity on a titanium alloy, Surface and Coatings Technology 200 (2006) 5581–5589.
[36] D. Aronov, R. Rosen, E.Z. Ron, G. Rosenman, Tunable hydroxyapatite wettability: effect on adhesion of biological molecules, Process Biochemistry 41 (2006) 2367–2372.
[37] B. Li, B.E. Logan, Bacterial adhesion to glass and metal-oxide surfaces, Colloids and Surfaces B: Biointerfaces 36 (2004) 81–90.